Projected Dipole Model for Quantum Plasmonics

Wei Yan,[1,2] Martijn Wubs,[1,2] and N. Asger Mortensen[1,2,3]

[1]*Department of Photonics Engineering, Technical University of Denmark, DK-2800 Kongens Lyngby, Denmark*
[2]*Center for Nanostructured Graphene, Technical University of Denmark, DK-2800 Kongens Lyngby, Denmark*
[3]*Institute of Applied Physics, Abbe Center of Photonics, Friedrich Schiller University Jena, Jena 07745, Germany*

Quantum effects of plasmonic phenomena have been explored through *ab initio* studies, but only for exceedingly small metallic nanostructures, leaving most experimentally relevant structures too large to handle. We propose instead an effective description with the computationally appealing features of classical electrodynamics, while quantum properties are described accurately through an infinitely thin layer of dipoles oriented normally to the metal surface. The nonlocal polarizability of the dipole layer—the only introduced parameter—is mapped from the free-electron distribution near the metal surface as obtained with 1D quantum calculations, such as time-dependent density-functional theory (TDDFT), and is determined once and for all. The model can be applied in two and three dimensions to any system size that is tractable within classical electrodynamics, while capturing quantum plasmonic aspects of nonlocal response and a finite work function with TDDFT-level accuracy. Applying the theory to dimers, we find quantum corrections to the hybridization even in mesoscopic dimers, as long as the gap itself is subnanometric.

Nanoscale metallic structures receive considerable attention for plasmon phenomena beyond classical electrodynamics [1–5]. In deep nanoscale structures, quantum effects manifest themselves [6]. Size-dependent plasmon energies of metallic particles, a common topic in condensed matter physics [7–11], has been revisited with new insights [1,2]. Dimers hosting angstrom-scale gaps are being investigated intensively in search of quantum-tunneling effects [3,4], though interpretations highlight both quantum tunneling [12] and semiclassical dynamics [13]. Time-dependent density-functional theory (TDDFT) allows explorations into the quantum regime [14–16], albeit limited to atomic-scale systems.

Here we focus on the mesoscopic scale that is typical for state-of-the-art experiments: too small to obey classical local-response approximation (LRA), but too large for an efficient quantum treatment. Plasmonics at this scale has so far been described with some success by semiclassical hydrodynamic Drude model (HDM) that exhibit nonlocal response [5,13,17–20] and by the quantum-corrected model (QCM) for gaps between metals [12]. It is, however, desirable to look beyond these models.

In this Letter, we present the projected dipole model (PDM), a theory predicting optical properties of mesoscopic plasmonic systems with TDDFT-level accuracy. Their quantum effects are captured by a zero-thickness projected dipole layer (PDL) onto the metal surface, see Fig. 1. The idea is partly inspired by Ref. [18], where a finite-thickness local layer represents the HDM nonlocal response. Here, we go beyond the HDM and capture quantum phenomena of a microscopic theory of choice, TDDFT. A crucial computational advantage of the PDL is that its inclusion is elegantly absorbed into boundary conditions at the interface.

Projected dipole layer.—We first introduce the PDL, the key concept of our model. To reproduce quantum results of the reflectivity of a planar metal-air interface at $x = 0$, we add an infinitely thin layer of dipoles to the corresponding interface. The response of this PDL is defined as $\mathbf{P}_{\mathrm{PDL}} = \epsilon_0 \alpha \hat{\mathbf{n}} \, \hat{\mathbf{n}} \cdot \mathbf{E}_{\mathrm{air}} \delta(x)$, where $\hat{\mathbf{n}}$ is the normal vector pointing outward the metal and $\mathbf{E}_{\mathrm{air}}$ is the electric field in the air region. The unknown polarizability α of the polarization field $\mathbf{P}_{\mathrm{PDL}}$ will be identified below, after further motivating our model. The semi-infinite metal at $x < 0$ that is in the electrostatic limit driven by an external electric potential $\phi_{\mathrm{ext}} = e^{i\mathbf{k}_\parallel \cdot \mathbf{s} + k_\parallel x}$, where $\mathbf{s} = y\hat{\mathbf{y}} + z\hat{\mathbf{z}}$, exhibits an induced electron density $\rho(x) = q_1 \delta(x)$ within the LRA. The induced electric potential in the air equals $-eq_1 e^{-k_\parallel x}/2k_\parallel$. By contrast, $\rho(x)$ spreads across the
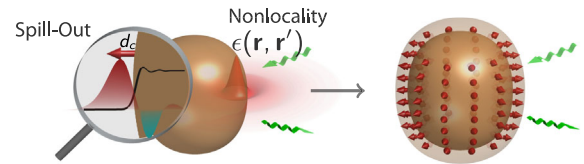

FIG. 1 (color online).   In the projected dipole model, light-driven quantum-plasmonic response in a metallic nanostructure (left) is represented in classical electrodynamics by an infinitely thin layer of dipoles that point perpendicularly to the surface (right). The loupe (left) highlights the spill-out of the microscopic electron distribution inducing a dipole moment proportional to the Feibelman parameter d_c.

interface in quantum theories. The induced electric potential consequently has a multipole expansion $(-eq_2 e^{-k_\parallel x}/2k_\parallel)[1 + k_\parallel d_c + O(k_\parallel^2 d_c^2)]$. Here the first and second terms in the bracket represent the monopole and dipole contributions, respectively, with $q_2 = \int dx\rho(x)$ and $d_c = \int dx x\rho(x)/q_2$ as the Feibelman parameter, i.e., the centroid of the induced charge. Clearly, the leading-order quantum effect is to induce a dipole moment proportional to d_c in the surface region. This motivates our choice of a PDL to capture quantum effects.

Planar surface polarizability.—Next we identify the polarizability of the PDL for the 1D planar metal-air interface (for dielectric surroundings, see [21]). Employing the TDDFT within the jellium approximation [22], we obtain the reflection coefficient $R_{KS}(k_\parallel, \omega)$ for the incident field. To require that the PDL system produces the same reflection, we have [23]

$$\alpha(\omega, k_\parallel) = \frac{[1 - R_{KS}(\omega, k_\parallel)] - \epsilon_m^{LRA}[1 + R_{KS}(\omega, k_\parallel)]}{k_\parallel \epsilon_m^{LRA}(\omega)[1 - R_{KS}(\omega, k_\parallel)]}, \quad (1)$$

where ϵ_m^{LRA} is the bulk permittivity of the metal. To interpret this result, we look into its long-wavelength $(k_\parallel \to 0)$ limit denoted as α_L. Since R_{KS} in this limit equals $-[\epsilon_m^{LRA}(\omega) - 1][1 + k_\parallel d_c(\omega)]/[\epsilon_m^{LRA}(\omega) + 1 - (\epsilon_m^{LRA}(\omega) - 1)k_\parallel d_c(\omega)]$ [31], we get $\alpha_L = [\epsilon_m^{LRA}(\omega) - 1]d_c(\omega)/\epsilon_m^{LRA}(\omega)$, which shows a direct relation between α_L and d_c as our intuitive expectation. Here d_c parameterizes two important quantum effects: electron spill-out via $Re[d_c]$ and electron-hole (*e-h*) excitations via $Im[d_c]$ [7]. Within the HDM, d_c becomes $-1/k_L$ ("spill-in" proper for noble metals [2,5] but not for simple metals [15,16]) in terms of the Thomas-Fermi wave number k_L [17], and $\alpha_L = (\epsilon_m^{LRA} - 1)/(\epsilon_m^{LRA} k_L)$, which is similar to the dielectric layer in Ref. [18]. The standard HDM cannot describe electron spill-out or *e-h* excitation, though; only recent HDM extensions include spill-out [19,32,33].

The plasmonic response of sodium exhibits an interplay between nonlocal response and spill-out due to a finite work function, and illustrates the potential of the PDM.
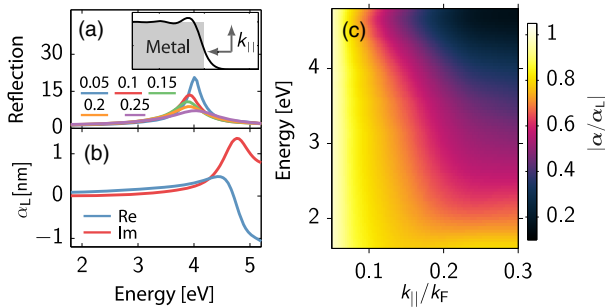

FIG. 2 (color online).   (a) TDDFT reflection spectra of a sodium surface for the electric field incidence with different $k_\parallel$ (in units of k_F) as illustrated in the inset. (b) Long-wavelength polarizability α_L. (c) Magnitude of polarizability α normalized by α_L.

Figure 2(a) shows reflection spectra off a planar sodium-air interface for different $k_\parallel$ by TDDFT. The peak around 4 eV corresponds to the surface plasmon (SP) resonance, which first redshifts and then blueshifts as $k_\parallel$ increases, while the width shows a broadening due to *e-h* excitations. Figure 2(b) depicts α_L, with around 4.8 eV a sign change of $Re[\alpha_L]$ and a peak in $Im[\alpha_L]$, which manifests the multipole surface plasmon resonance [8]. Figure 2(c) exhibits an increased $k_\parallel$ dependence of α for larger energies, so α_L is a good approximation only at low energies.

Arbitrary structures.—With the planar polarizability $\alpha(\omega, k_\parallel)$ as the input parameter of the theory, we here generalize it for an arbitrary structure. We seek the polarizability in real space, which for the planar surface is given by the inverse Fourier transform of $\alpha(\omega, k_\parallel)$, and holds a nonlocal form $\alpha_p(\omega, |\mathbf{s} - \mathbf{s}'|)$. As observed in Fig. 2(c), α is nearly constant for $k_\parallel < k_c \simeq 0.1 k_F$. Thus, the nonlocal range of α_p is of the order $1/k_c \simeq 1$ nm. For a curved surface with its curvature exceeding the 1-nm scale, we safely assume that the polarizability has the same expression as α_p, with the distance defined as the length of the shortest path between two points on the PDL, i.e., the shortest geodesic [24]. We thus obtain

$$\alpha(\omega, \mathbf{s}, \mathbf{s}') = \alpha_p(\omega, |\mathbf{s} - \mathbf{s}'|_{sg}). \quad (2)$$

Here, $|\mathbf{s} - \mathbf{s}'|_{sg}$ represents the length of the shortest path between $\mathbf{s}$ and $\mathbf{s}'$ on the PDL. We note that in Eq. (2), possible quantum size effects, i.e., the quantization of the electronic bands due to the confinement of the electron gas, are not taken into account. In metals, such effects are only pronounced when the confinement size approaches 1 nm [34].

In the LRA, the key parameter is ϵ_m^{LRA}. Including the quantum freedoms, we show that an additional parameter α is needed. Accordingly, the predictive power of the PDM is subject to the accuracy of the underlying *ab initio* theory (in our case, TDDFT). Potentially, α might even be obtained through experiments, with tabulations for different metals similar to the common practice for ϵ_m^{LRA}. The presence of the PDL is equivalent to the boundary condition connecting the electric fields in the metal and air regions with $\mathbf{E}_{\parallel,air}(\mathbf{s}) - \mathbf{E}_{\parallel,metal}(\mathbf{s}) = -\nabla_\mathbf{s} \int d\mathbf{s}' \alpha(\omega, \mathbf{s}, \mathbf{s}')\hat{\mathbf{n}}(\mathbf{s}') \cdot \mathbf{E}_{air}(\mathbf{s}')$ [23]. Here the subscript "$\parallel$" represents the tangential components and the operator ∇_s gives the gradient components in the tangential directions of the boundary. The discontinuity of the parallel electric fields across the boundary is a direct manifestation of the PDL, which squeezes the spatial information of the microscopic electron distribution into a zero-thickness layer. The boundary condition can be conveniently adopted in numerical computations, and its convolution integral is similar in form to the Green's function integral in classical electrodynamics. As such, it introduces no extra complications. If large

momentum fields do not contribute to the dynamics significantly, α can be approximated by the local form $\alpha_L(\omega)\delta(\mathbf{s}-\mathbf{s}')$ with the simplified boundary condition $\mathbf{E}_{\parallel,\text{air}} - \mathbf{E}_{\parallel,\text{metal}} = -\alpha_L\boldsymbol{\nabla}_s(\hat{\mathbf{n}}\cdot\mathbf{E}_{\text{air}})$ [23]. Below, we use Eq. (2).

Benchmarks against TDDFT.—We confirm the validity of the PDM for a sodium dimer of two identical cylindrical nanowires excited by an electric field along the gap. In Fig. 3(a), we present the extinction spectra predicted by LRA, PDM, and TDDFT with a nanowire of radius 4.9 nm and gap 0.74 nm. The local bulk permittivity is $\epsilon_{\text{metal}}^{\text{LRA}} = 1 - \omega_p^2/\omega(\omega+i\gamma)$, where $\omega_p = 5.89$ eV, $\gamma = 0.085$ eV for the PDM, and $\gamma = 0.16$ eV for the LRA [15]. The PDM and TDDFT spectra agree with each other quantitatively, and both predict that the SP peak redshifts with respect to the LRA one, and that the resonance is broadened. The latter phenomenon can be qualitatively captured by the generalized nonlocal optical response [13] via the diffusive scattering of the surface current, while the redshift of the resonance requires for the accounting of electron spill-out [15,16].

As the size of the electron system decreases, surface curvature and quantum size effects may challenge the assumptions behind the PDM. Considering the nanowire dimer with 2-nm radius and 1-nm gap, we plot the extinction spectra in Fig. 3(b). The PDM results still agree surprisingly well with TDDFT spectra. Furthermore, as one of our main results we find that the PDM and TDDFT spectra agree well, despite the fact that the PDM models both metal-air interfaces in an independent surface approximation (ISA).

The multiscale dimer system with a subnanometer gap distance introduces an additional small scale for hosting the quantum effects [14,35]. Such a setup is usually challenging for *ab initio* studies, especially for 3D systems. However, the PDM can be applied efficiently. Figure 3(c) depicts the color map of the extinction cross section predicted by the PDM for the 3D sodium spherical dimer with particle radius ranging from 3 to 23 nm and with a gap of 0.74 nm. To demonstrate the quantum effects of a typical multiscale system, Fig. 3(d) plots the extinction spectra at the 20-nm radius of Fig. 3(c) (dash-dot line), contrasting the PDM and LRA results. Similar to Figs. 3(a) and 3(b), quantum effects manifest themselves by shifting and broadening the SP resonances. Interestingly, the higher-order modes in this case are less affected by quantum effects, since plasmon fields in larger structures are less confined.

More gap effects.—In the PDM, we invoked the ISA and thus only included quantum effects related to a single metal surface. When the gap between two metal surfaces approaches the d_c scale, the significant wave function overlap of the two surfaces should be taken into account. An intuitive way is to treat the gap as an effective medium, as introduced in the QCM with a Drude permittivity, to mimic the dissipation associated with quantum tunneling (QT) [12]. To promote the PDM for the smallest gaps, here we present an unambiguous extraction of the effective gap permittivity from TDDFT calculations, instead of relying on the assumption that QT is the cause of all gap-related dissipation.

Turning from the spectral to the spatial information provided by TDDFT, we extract the effective local permittivity ϵ_{eff} defined as $D/[\epsilon_0 E]$. In Fig. 4(a) we visualize
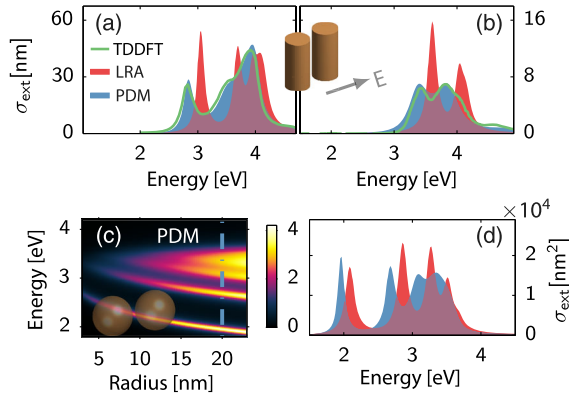

FIG. 3 (color online). Extinction properties of sodium dimers within LRA, PDM, and TDDFT for (a) cylindrical wire with radius 4.9 nm and gap 0.74 nm, (b) cylindrical wire with radius 2 nm and gap 1 nm, (c) spherical particle with radius varying from 3 to 23 nm and with 0.74-nm gap distance, where the extinction cross sections are normalized by the surface area of the sphere, and (d) the 20-nm radius case [dash-dotted line in (c)]. TDDFT results in (a) and (b) are reproduced from Refs. [15] and [16], respectively.
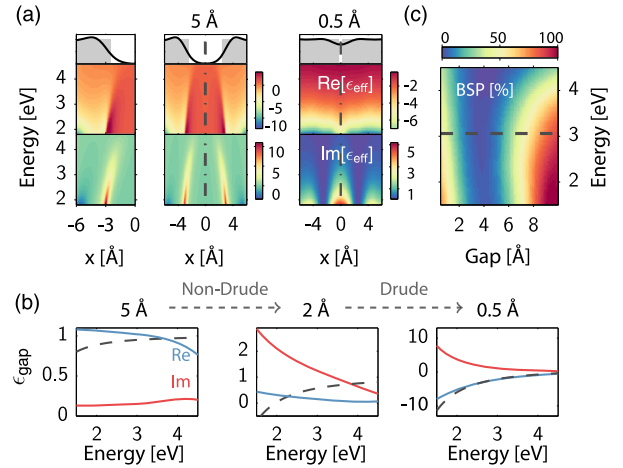

FIG. 4 (color online). Gap effects for planar sodium-vacuum-sodium gap structures within TDDFT. (a) Effective permittivity for a single interface and for 5 and 0.5 Å gaps. (b) Frequency dependence of the corresponding midgap effective permittivities. Dashed lines indicate the lossless Drude model, with its plasma frequency determined by the midgap equilibrium electron density. (c) Electron-hole backward scattering proportion (BSP) as a function of gap distance and energy.

ϵ_{eff} for a single interface and for two gap distances, 5 and 0.5 Å. For the 5-Å gap case, two separated metallic systems can be identified, as seen from the clear boundaries between the negative- and positive-valued regions of Re[ϵ_{eff}], as well as for the single interface. Furthermore, the loss Im[ϵ_{eff}] peaks right at the interfaces where we likewise have Re[ϵ_{eff}] ~ 0. The dissipation (associated with *e-h* excitations) occurs around the metal surface, in agreement with mesoscopic transport theory [36]. By contrast, for the 0.5-Å gap no definite boundary of the two metals can be observed from the equilibrium electron density. The induced electron current at the gap center is, accordingly, the classical Drude current. In the optical spectra this regime (gaps of 1–2 Å and below) is characterized by a transition from the bonding-dipole plasmon (BDP) resonance to the charge-transfer plasmon (CTP).

Figure 4(b) shows midgap properties, $\epsilon_{\text{gap}} = \epsilon_{\text{eff}}(x = 0)$, for gaps of 5, 2, and 0.5 Å. In general, we anticipate a transition from non-Drude (quantum) response to Drude (classical) response as the gap reduces. Indeed, for the 0.5-Å gap the midgap response is captured by the classical Drude model (dashed line) [37]. On the other hand, the larger separation of 5 Å shows a completely non-Drude behavior. The 2-Å gap exhibits almost frequency-independent Re[ϵ_{gap}], thus constituting the crossover gap size between non-Drude and Drude responses.

Modeling Å-sized gaps.—We will now discuss how in the PDM a dimer gap can be treated as an effective medium [12], thereby accounting for not only quantum effects of individual metal interfaces but also for their strong mutual proximity. The procedure in this projected dipole gap model (PDGM) is to treat the gap as an effective medium with permittivity ϵ_{gap} (extracted from TDDFT) within the PDM. To illustrate the accuracy of the PDGM, we consider a nanowire dimer of two sodium cylinders with radius 4.9 nm driven by a uniform electric field along the gap. In Fig. 5 we illustrate the extinction spectra as the gap distance decreases from 5.3 to 0 Å (contact). As expected, not all LRA resonances are supported by the more accurate TDDFT calculations. The PDM captures the broadening of the resonance as the gap reduces, with spectra closely resembling those of TDDFT. However, the PDM neglects gap effects, and, therefore, underestimates the resonance broadening. For the same reason the CTP does not appear before physical contact. Turning to the PDGM, we find almost perfect agreement with the TDDFT spectra, even for the smallest gaps.

Discussion.—The great accuracy of the PDM in Fig. 3 and of the PDGM in Fig. 5 calls for a discussion of the dissipative quantum processes at interfaces and near gaps. The TDDFT calculations account for plasmon damping due to *e-h* excitations. To interpret our results, we identify two scattering processes: an electron state propagating towards the interface or gap can create *e-h* pairs in forward or backward scattering. For a single interface, at energies
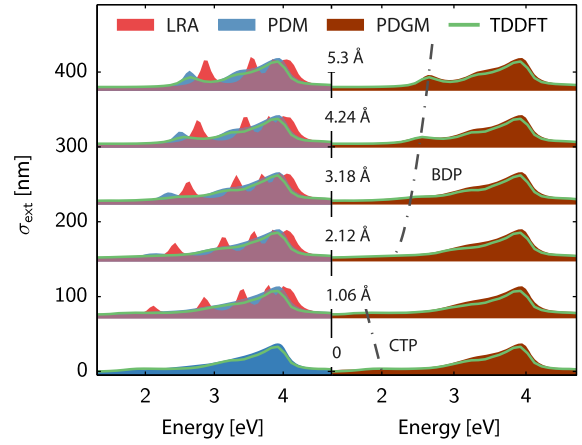

FIG. 5 (color online). Extinction cross sections of a cylindrical sodium nanowire dimer with radius 4.9 nm, for gaps decreasing from 5.3 to 0 Å. Comparison of predictions by LRA, TDDFT, PDM, and PDGM. TDDFT spectra originate from Ref. [15].

below the work function all dissipation due to *e-h* creation is associated with backward scattering, while forward scattering exists above the work function. In contrast, for a dimer structure with a narrow gap, forward scattering below the work function is permitted. The PDM assumes all gap- and interface-related loss to be due to backward scattering, whereas the QCM calculates all gap-related loss as due to QT, i.e., forward scattering [12]. Finally, the PDGM does not systematically exclude one or both processes. Thus, the question is whether forward or backward scattering dominates *e-h* creation.

Figure 4(c) depicts the *e-h* backward scattering proportion (BSP) [23], defined as the ratio between the backward and total scattering rates, for two vacuum-gapped planar sodium surfaces excited by a uniform electric field. The BSP exhibits completely different behavior depending on the gap sizes. For gaps > 7 Å, the BSP approaches 100% below the work function (dashed line), which explains the validity of the PDM in Fig. 3. For smaller gaps, down to 3 Å, the BSP continuously decreases. Below the work function this is due to QT, and should relate with the lowered energy barrier, which eases the *e-h* excitations across the gap for high energies. As the gap shrinks further below 3 Å, the concept of QT is not well defined, since the vacuum gap separating different systems cannot be unambiguously defined. Accordingly, the BSP starts *increasing* when gaps are smaller than 3 Å, and eventually dominates the forward scattering at low energies.

In conclusion, we propose a projected dipole model for quantum plasmonics, where the quantum response is represented within the framework of classical electrodynamics by a zero-thickness dipole layer. We have shown that the PDM can predict quantum plasmonic aspects of nonlocal response and a finite work function with TDDFT-level accuracy. In addition to the demonstrated extinction spectra, the PDM works equally well for the near-field

properties [23]. Our work also provides insights into the possible importance of optical tunneling currents in plasmonic dimers. Finally, our results have great potential for multiscale modeling in computational plasmonics, where quantum effects can now be accurately explored even in large systems.

[1] J. A. Scholl, A. L. Koh, and J. A. Dionne, Nature (London) **483**, 421 (2012).

[2] S. Raza, N. Stenger, S. Kadkhodazadeh, S. V. Fischer, N. Kostesha, A.-P. Jauho, A. Burrows, M. Wubs, and N. A. Mortensen, Nanophotonics **2**, 131 (2013).

[3] K. J. Savage, M. M. Hawkeye, R. Esteban, A. G. Borisov, J. Aizpurua, and J. J. Baumberg, Nature (London) **491**, 574 (2012).

[4] S. F. Tan, L. Wu, J. K. W. Yang, P. Bai, M. Bosman, and C. A. Nijhuis, Science **343**, 1496 (2014).

[5] C. Ciracì, R. T. Hill, J. J. Mock, Y. Urzhumov, A. I. Fernández-Domínguez, S. A. Maier, J. B. Pendry, A. Chilkoti, and D. R. Smith, Science **337**, 1072 (2012).

[6] M. S. Tame, K. R. McEnery, S. K. Oezdemir, J. Lee, S. A. Maier, and M. S. Kim, Nat. Phys. **9**, 329 (2013).

[7] P. J. Feibelman, Prog. Surf. Sci. **12**, 287 (1982).

[8] A. Liebsch, Phys. Rev. B **48**, 11317 (1993).

[9] P. Apell and D. R. Penn, Phys. Rev. Lett. **50**, 1316 (1983).

[10] J. Tiggesbäumker, L. Köller, K. H. Meiwes-Broer, and A. Liebsch, Phys. Rev. A **48**, R1749 (1993).

[11] K. P. Charlé, L. König, S. Nepijko, I. Rabin, and W. Schulze, Cryst. Res. Technol. **33**, 1085 (1998).

[12] R. Esteban, A. Borisov, P. Nordlander, and J. Aizpurua, Nat. Commun. **3**, 825 (2012).

[13] N. A. Mortensen, S. Raza, M. Wubs, T. Sondergaard, and S. I. Bozhevolnyi, Nat. Commun. **5**, 3809 (2014).

[14] D. Marinica, A. Kazansky, P. Nordlander, J. Aizpurua, and A. Borisov, Nano Lett. **12**, 1333 (2012).

[15] T. V. Teperik, P. Nordlander, J. Aizpurua, and A. G. Borisov, Phys. Rev. Lett. **110**, 263901 (2013).

[16] L. Stella, P. Zhang, F. García-Vidal, A. Rubio, and P. García-González, J. Phys. Chem. C **117**, 8941 (2013).

[17] S. Raza, G. Toscano, A.-P. Jauho, M. Wubs, and N. A. Mortensen, Phys. Rev. B **84**, 121412(R) (2011).

[18] Y. Luo, A. I. Fernández-Domínguez, A. Wiener, S. A. Maier, and J. B. Pendry, Phys. Rev. Lett. **111**, 093901 (2013).

[19] C. David and F. J. García de Abajo, ACS Nano **8**, 9558 (2014).

[20] S. Raza, S. I. Bozhevolnyi, M. Wubs, and N. A. Mortensen, J. Phys. Condens. Matter **27**, 183204 (2015).

[21] D. Jin *et al.*, arXiv:1504.07867.

[22] *Time-Dependent Density Functional Theory*, Lecture Notes in Physics Vol. 706, edited by M. A. L. Marques, C. A. Ullrich, F. Nogueira, A. Rubio, K. Burke, and E. K. U. Gross (Springer, Berlin, 2006).

[23] See Supplemental Material at http://link.aps.org/supplemental/10.1103/PhysRevLett.115.137403, which includes Refs. [2,5,12,13,15,16,22,24,25–30].

[24] U. Leonhardt and T. G. Philbin, Prog. Opt. **53**, 69 (2009).

[25] W. Yan, N. A. Mortensen, and M. Wubs, Phys. Rev. B **88**, 155414 (2013).

[26] N. Lang and W. Kohn, Phys. Rev. B **1**, 4555 (1970).

[27] R. Kimmel and J. A. Stehian, Proc. Natl. Acad. Sci. U.S.A. **95**, 8431 (1998).

[28] H. Bruus and K. Flensberg, *Many-Body Quantum Theory in Condensed Matter Physics: An Introduction* (Oxford University Press, Oxford, 2004).

[29] F. J. García de Abajo and A. Howie, Phys. Rev. Lett. **80**, 5180 (1998).

[30] T. V. Teperik, P. Nordlander, J. Aizpurua, and A. G. Borisov, Opt. Express **21**, 27306 (2013).

[31] K. D. Tsuei, E. W. Plummer, A. Liebsch, E. Pehlke, K. Kempa, and P. Bakshi, Surf. Sci. **247**, 302 (1991).

[32] G. Toscano, J. Straubel, A. Kwiatkowski, C. Rockstuhl, F. Evers, H. Xu, N. A. Mortensen, and M. Wubs, Nat. Commun. **6**, 7132 (2015).

[33] W. Yan, Phys. Rev. B **91**, 115416 (2015).

[34] R. C. Monreal, T. J. Antosiewicz, and S. P. Apell, New J. Phys. **15**, 083044 (2013).

[35] S. Raza, M. Wubs, S. I. Bozhevolnyi, and N. A. Mortensen, Opt. Lett. **40**, 839 (2015).

[36] S. Datta, *Electronic Transport in Mesoscopic Systems* (Cambridge University Press, Cambridge, England, 1995).

[37] M. Ichikawa, J. Phys. Soc. Jpn. **80**, 044606 (2011).